Interface-Driven Ferromagnetism within the Quantum Wells of a Rare Earth Titanate Superlattice

R. F. Need,[1] B. J. Isaac,[1] B. J. Kirby,[2] J. A. Borchers,[2] S. Stemmer,[1] and Stephen D. Wilson[1,*]

[1]*Materials Department, University of California, Santa Barbara, California 93106-5050, USA*
[2]*NIST Center for Neutron Research, National Institute of Standards and Technology, Gaithersburg, Maryland 20899-6100, USA*

Here we present polarized neutron reflectometry measurements exploring thin film heterostructures composed of a strongly correlated Mott state, $GdTiO_3$, embedded with $SrTiO_3$ quantum wells. Our results reveal that the net ferromagnetism inherent to the Mott $GdTiO_3$ matrix propagates into the nominally nonmagnetic $SrTiO_3$ quantum wells and tracks the magnetic order parameter of the host Mott insulating matrix. Beyond a well thickness of 5 SrO layers, the magnetic moment within the wells is dramatically suppressed, suggesting that quenched well magnetism comprises the likely origin of quantum critical magnetotransport in this thin film architecture. Our data demonstrate that the interplay between proximate exchange fields and polarity-induced carrier densities can stabilize extended magnetic states within $SrTiO_3$ quantum wells.

Interfaces between $RETiO_3$ (RE = Gd, Sm, etc.) and $SrTiO_3$ aggregate charge via a polar discontinuity between the differing valence states intrinsic to the rare earth and alkali earth layers of the two compounds [1]. In multilayer films, two sequential interfaces define a quantum well into which the polarization-induced carriers preferentially spread [1,2]. This induced charge lives in a physically rich landscape, one where traversing between sufficiently thick layers also necessitates the relaxation of d-electron orbital polarization, long-range magnetic order, and strong on-site Coulomb interactions [3]. The thickness of the quantum well also defines a length scale for the mediation of interactions between polarity-induced carriers, which at sufficiently high densities have the potential to drive electronic order [4]. Adding further complexity, structural symmetries (i.e., oxygen octahedral tilts) from the parent $RETiO_3$ can coherently propagate across the interface and into the well before relaxing beyond a critical thickness [5–7]. Ultimately, the combination of these effects may modify the bandwidth and electronic states manifest within the well, generating a parameter space not realizable in bulk form.

The interplay between polar interface charge and a proximate correlated state renders exotic transport phenomena in $SmTiO_3/SrTiO_3$ and $GdTiO_3/SrTiO_3$ heterostructures [8,9]. The band insulator $SrTiO_3$, when embedded as thin quantum wells within Mott insulating $GdTiO_3$ barriers, exhibits metallic transport mediated via interface carriers [10]. A metal-to-insulator transition emerges as the well thickness (defined by the number of SrO layers) decreases to 2 SrO layers and the corresponding well carrier density diverges [11]. Prior to this metal-to-insulator transition, $SrTiO_3$ quantum wells with thicknesses of approximately 3 SrO layers display an unusual

hysteresis in their low temperature longitudinal magneto-resistance—a state suggestive of domain switching and a field coupled electronic order parameter [12,13].

Intriguingly, a divergent carrier mass was also observed near the stabilization of this order parameter, consistent with a quantum critical point driven by the well carrier density or dimensionality [11]. However, little remains understood regarding the origins of this unusual phase behavior in $GdTiO_3/SrTiO_3$ heterostructures absent a direct resolution of the order parameter within the wells. Addressing this and searching for the presence of interface-induced magnetic order requires access to an experimental probe sensitive to magnetic polarization and capable of resolving its depth profile throughout a heterostructure—both of which are achievable via polarized neutron reflectometry (PNR) [14–16].

In this Letter, we present a PNR study exploring magnetic order within the quantum wells of $GdTiO_3/SrTiO_3$ heterostructures. Our data reveal the presence of magnetization induced within the $SrTiO_3$ wells below a critical well thickness of 5 SrO and demonstrate a novel realization of magnetic order induced within a nonmagnetic medium through the interplay between polarity-induced charge density and proximity-induced magnetic exchange. Furthermore, our results suggest that well magnetism represents the local order parameter whose suppression generates the divergent carrier mass reported in earlier magnetotransport studies [11].

A series of superlattice films containing a quintuple of 4 nm $GdTiO_3$ spacer layers separated by variable width $SrTiO_3$ quantum wells (2 SrO, 3 SrO, 5 SrO, and 10 SrO layers) were grown via molecular beam epitaxy, and PNR measurements were collected at the NIST Center for Neutron Research on the PBR reflectometer. PNR models

of magnetism in $GdTiO_3/SrTiO_3$ heterostructures benefit from independent measurements of the films' structures in order to constrain the number of free parameters. To achieve this, structural profiles were collected via room temperature x-ray reflectivity measurements [17], and the x-ray reflectivity layer thicknesses and effective roughnesses were used as a fixed input in subsequent PNR models. Further details regarding film growth and reflectometry experiments are provided in Supplemental Material [17] and detailed electron microscopy characterization of the film interfaces is described elsewhere [2,5,10]. While transmission electron microscopy (TEM) measurements of identical superlattice films show sharp interfaces [2,5,10] and a maximum chemical intermixing of one atomic layer [10], roughnesses measured by reflectivity are an average across the entire sample surface area, including effects from step edges across the underlying substrate. Hence, modeling quantum wells in the thin layer limit renders widths, roughnesses, and scattering length densities (SLDs) whose values become intrinsically coupled. As such, the refined roughness values in the thin well limit do not have an independent physical meaning and should not be compared to local probe measurements (e.g., TEM).

Figure 1 shows the results from low temperature ($T = 4$ K) PNR measurements on four superlattice samples collected under a field-cooled state ($\mu_0 H = 0.7$ T). Solid
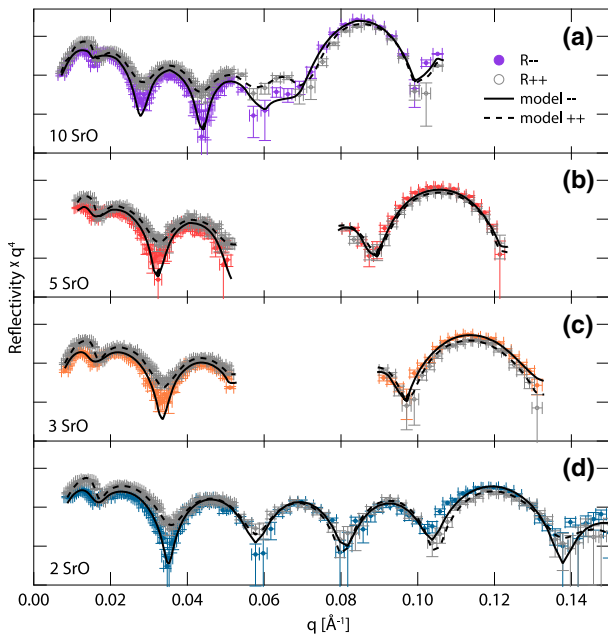
and empty symbols show non-spin-flip data collected for specular reflectivity curves with the incident and scattered neutron polarizations oriented down (R^{--}) and up (R^{++}) relative to the sample field, respectively, both of which encode information regarding the nuclear and magnetic SLD profiles of the film [22,23]. While the overall oscillation of both curves is primarily reflective of the chemical profile of the film, splitting between these curves denotes a net, in-plane, magnetic polarization along the field direction where changes in magnetization between layers produce a difference in the ($R^{++} - R^{--}$) cross section. Chemical and magnetic scattering profiles can be modeled simultaneously via an optical matrix formalism [17,24], and the resulting fits are plotted in Fig. 1. Gaps in the data sets [i.e., $q = 0.055$–0.080 Å^{-1} in Figs. 1(b) and 1(c)] are due to limited measurement time and prioritization of q ranges where $SrTiO_3$ features are most salient.

The parameters summarizing the modeled films' depth profiles at 4 and 30 K are plotted in Fig. 2. Chemical contrast varies as expected between $GdTiO_3$ and $SrTiO_3$ layers with the topmost $GdTiO_3$ layer distinct from the buried layers due to brief periods of exposure to

FIG. 1. PNR data of $GdTiO_3/SrTiO_3$ superlattice films. (a)–(d) Neutron reflectivity as a function of momentum transfer for $GdTiO_3/SrTiO_3/GdTiO_3$ superlattice structures with quantum wells of thickness 10 SrO, 5 SrO, 3 SrO, and 2 SrO layers, respectively. Open gray symbols denote the R^{++} cross section and closed color symbols denote R^{--}. Dashed lines (R^{++}) and solid lines (R^{--}) indicate the fits resulting from structural and magnetic models of the data.
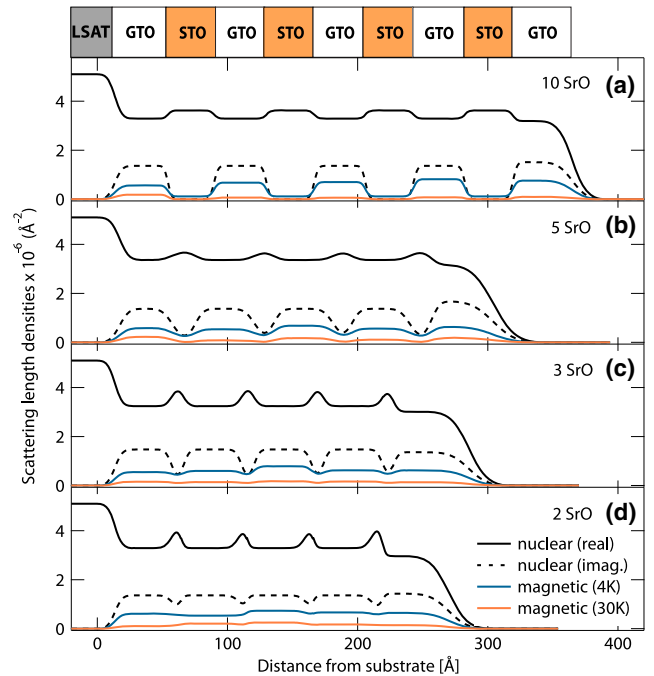

FIG. 2. Nuclear and magnetic depth profiles of $GdTiO_3/SrTiO_3$ superlattice films. SLDs as a function of film depth corresponding to the structural and magnetic models of PNR data for superlattice films with (a) 10 SrO, (b) 5 SrO, (c) 3 SrO, and (d) 2 SrO layers thick $SrTiO_3$ wells. Solid and dashed black lines correspond to the real and imaginary components of nuclear scattering density profile, while the blue and orange lines correspond to the magnetization fits at $T = 4$ and 30 K. The sequence of $GdTiO_3$ (GTO) and $SrTiO_3$ (STO) layers grown on the $(La_{0.3}Sr_{0.7})(Al_{0.65}Ta_{0.35})O_3$ (LSAT) substrate is illustrated above the plots.

atmosphere. The effective roughnesses of the GdTiO₃ →
SrTiO₃ and SrTiO₃ → GdTiO₃ interfaces span the thicknesses of the wells in the 2 SrO and 3 SrO samples;
however, the wells in the 5 SrO and 10 SrO samples are
able to reach their nominal bulk SLDs and increasingly
decouple from neighboring layers. To better isolate magnetism in the wells, nuclear SLDs were refined at low
temperature and then fixed [17]; only the magnetic neutron
SLDs were allowed to vary as a function of temperature.

The magnetic contrast between neighboring layers at 4 K
notably does not follow the expected contrast between
ferrimagnetic and nonmagnetic layers. Instead, a finite
magnetization persists across the SrTiO₃ wells for the 2
SrO, 3 SrO, and 5 SrO samples. To better demonstrate this,
the magnetic components of the total scattering profiles
are isolated by plotting the spin asymmetries $(R^{++} -
R^{--})/(R^{++} + R^{--})$ in Fig. 3. Here, the low-q portion of
the asymmetry is dominated by the ferrimagnetism of
GdTiO₃ spacers comprising the bulk of the sample. At
higher q values, the scattering is more sensitive to magnetism associated with the SrTiO₃ quantum wells, particularly
at a thickness-dependent Bragg position of the bilayer
repeat. Modeling the combination of these two extremes
allows for the magnetic contrast between the layers to be
directly refined.

A qualitative sense of magnetism inside the thinnest
2 SrO wells is apparent via inspection of Figs. 1(d), 2(d),
and 3(d). Figure 1(d) illustrates the Bragg peak and the
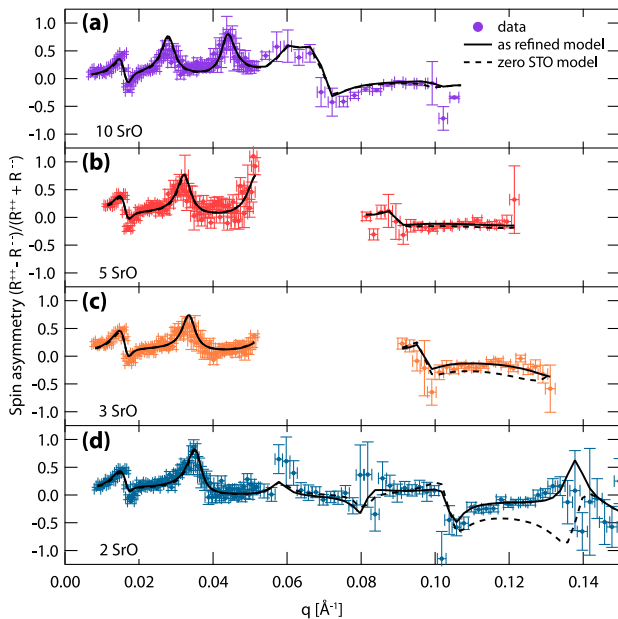corresponding R^{++} and R^{--} cross sections associated with

the bilayer repeat at $q \approx 0.12$ Å⁻¹. The model profiles
corresponding to these reflectivity curves plotted in
Fig. 2(d) show sharp contrast between the nuclear SLDs;
however, nearly negligible contrast is apparent within the
magnetizations between layers. In order to account for this
diminished magnetic contrast, the presence of magnetism
within the SrTiO₃ wells is illustrated in Fig. 3(d). Here, a
model of spin asymmetry allowing magnetized SrTiO₃
wells is compared with one forcing the magnetization
contribution from SrTiO₃ to zero in the well center. The
freely refined model, placing finite magnetization in the
SrTiO₃ wells, matches the data substantially better in
the high-q limit where sensitivity to SrTiO₃ is maximal.
Stated in other words, spin asymmetry values near zero in
the region of the Bragg peak necessitate a model with
magnetism in the SrTiO₃ wells in order to produce the
muted magnetic scattering contrast in the data.

The average magnetization values in each superlattice
(collected at the layer center values in model profiles) are
plotted as a function of temperature for the four buried
GdTiO₃ and SrTiO₃ layers in Figs. 4(a) and 4(b), respectively. Looking first at the spacer GdTiO₃ layers, ordered
moment values show a temperature dependence tracking
that of the ferrimagnetic order parameter observed in bulk
crystals and relaxed films [25–27]. The small amount of
scatter in the data arises from ambiguities in the absolute
normalization of the reflectivity data [17], and taken as an
average, the moments observed in the GdTiO₃ layers are
$1.42 \pm 0.20\mu_B$/f.u. at 4 K and $0.33 \pm 0.11\mu_B$/f.u. at 30 K
(f.u. is formula unit). In order to confirm that the GdTiO₃
magnetization is independent of the well thicknesses, a
separate film composed of only a single 5 nm layer of
GdTiO₃ was measured under identical conditions (i.e.,
$\mu_0 H = 0.7$ T field cooled). The magnetization was refined
to be 1.43 ± 0.13 and $0.24 \pm 0.19\mu_B$/f.u. at 4 and 30 K,
respectively—within error of the superlattice values [17].
The agreement between the magnetic properties of the
isolated thin film and GdTiO₃ spacer layers confirms that
the GdTiO₃ spacer layers are thick enough to decouple
from the SrTiO₃ quantum wells. This allows for added
confidence in isolating the evolution of SrTiO₃ magnetism
under varying well thickness.

The magnetization values inherent to the SrTiO₃ layers
are plotted in Fig. 4(b). For the three thinnest wells (2 SrO,
3 SrO, and 5 SrO), SrTiO₃ layers exhibit a finite magnetization whose temperature dependence seemingly tracks
that of the polarizing GdTiO₃ spacer layers. The saturated
(4 K) moments in the SrTiO₃ layers increase as the well
thicknesses are decreased and the electron gas at the
interfaces is further confined, eventually reaching a peak
value $1.11 \pm 0.11\mu_B$/f.u. in the center of the 2 SrO wells.
This value is within error of the $1\ \mu_B$/Ti naively expected
for fully polarized $S = 1/2$ Ti³⁺ moments. In contrast, the
thickest 10 SrO sample refines to show a nearly vanishing
SrTiO₃ magnetic moment within resolution ($0.25\ \mu_B$/f.u.

FIG. 3.   Spin asymmetry at $T = 4$ K in GdTiO₃/SrTiO₃ super-
lattice films with (a) 10 SrO, (b) 5 SrO, (c) 3 SrO, and (d) 2 SrO
layers thick SrTiO₃ wells. Solid lines represent the refined
models to the data, and the dashed lines represent a model
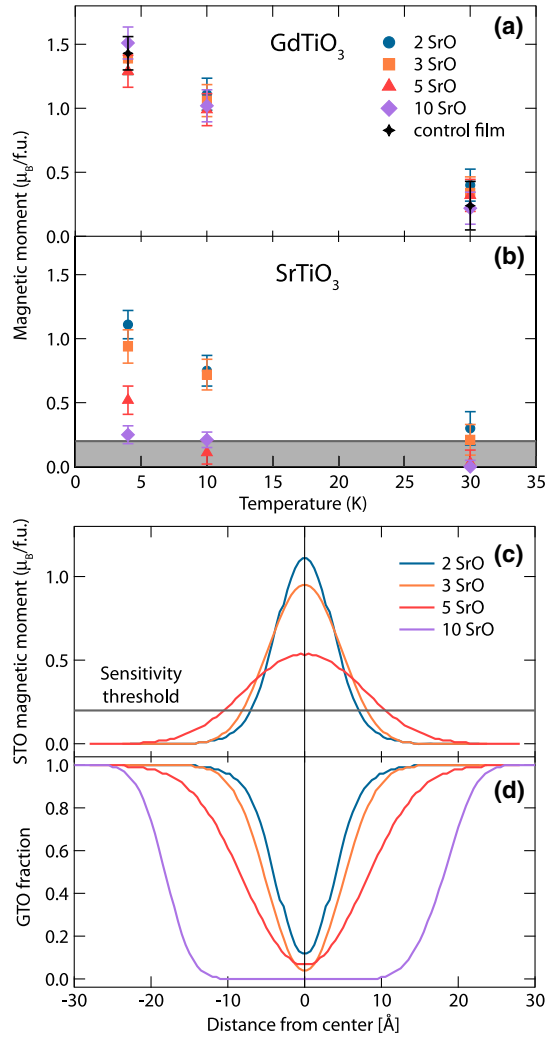constraining zero magnetization contribution from SrTiO₃.

FIG. 4. (a) Magnetic moment per formula unit in $GdTiO_3$ layers plotted as a function of temperature for both superlattice films and the reference $GdTiO_3$ film as described in the text. (b) Magnetic moment per formula unit observed within $SrTiO_3$ layers plotted as a function of temperature in superlattice films. Shaded region denotes approximate experimental sensitivity to $SrTiO_3$ moments. (c) Effective magnetization profiles for quantum wells after removing convolved $GdTiO_3$ contributions. (d) The relative fraction of $GdTiO_3$ convolved within the quantum wells as a function of distance from the well center.

at 4 K). Here, the experimental sensitivity is effectively constrained by the uncertainty in the magnetization of the $GdTiO_3$ layers at this temperature. This is illustrated in Fig. 3(a) where models of the spin asymmetry containing magnetic versus nonmagnetic $SrTiO_3$ layers are identical.

In order to parametrize the magnetism native to the quantum wells, the contribution of $GdTiO_3$ moments to the apparent magnetization of the $SrTiO_3$ wells can be largely accounted for and removed [15]. Specifically, the concentration of $GdTiO_3$ apparent within the wells can be calculated from the real parts of the nuclear SLD profiles by interpolating between pure $GdTiO_3$ and pure $SrTiO_3$.

This average convolution between layers is plotted in Fig. 4(d) and represents the fraction of $GdTiO_3$ convolved into the $SrTiO_3$ layers as a function of displacement from the center of the wells. In the thickest 10 SrO wells, the $GdTiO_3$ fraction drops to zero throughout the majority of the well, whereas in the thinnest 2 SrO wells, the apparent roughness mixes in a substantial fraction of $GdTiO_3$ close to the well center. This effective profile of $GdTiO_3$ within the wells can then be multiplied by the magnetization inherent to these spacer layers, yielding a maximum magnetic contribution from $GdTiO_3$ throughout the depth of the well. The $GdTiO_3$ contribution is then subtracted from the total refined $SrTiO_3$ magnetization profile (cf. Fig. 2), and the result is plotted in Fig. 4(c). This subtracted profile gives an average sense of how much of the refined moment is attributable to electrons induced within the well by the polar discontinuities.

The intrinsic ferromagnetism within the $SrTiO_3$ layers necessarily originates via the high-density two-dimensional electron gas (2DEG) induced at the interfaces. Half of an electron per area unit cell is contributed to each well via the top and the bottom interfaces, yielding a total of one electron per well [28]. Therefore, the integrated polarized moment in each well should be a constant value of 1 μ_B regardless of the well thickness. From our models, we calculate total integrated moments in the wells to be 2.75, 2.83, and 2.60 μ_B per well, for the 2, 3, and 5 SrO samples, respectively. Although these values are consistent with a picture of a constant integral moment, their magnitude likely reflects an inherent overestimation born by modeling the magnetization density as peaked in the center of the $SrTiO_3$ wells [17].

While f-d hybridization effects may play a role in polarizing some fraction of electrons directly at the interfaces, the majority of induced electrons are known to substantially delocalize into the volume of the $SrTiO_3$ wells and suggest a more extended exchange mechanism [2]. The density of interface-induced carriers nominally decays by 50% over approximately 1 nm into the bulk of $SrTiO_3$ [13], and the average 1.8 nm thick wells of the 5 SrO sample are consistent with a threshold where the overlap between interface states becomes appreciable. Moving substantially above this thickness corresponds to distances where the extended 2DEGs stabilized at each polar interface no longer sufficiently overlap and support the continuation of the exchange field across the well. We stress here, however, that our PNR measurements are unable to comment on the presence of magnetic texture within the wells themselves; rather, in the thin well limit, the resolution of our data only permits effective models of uniformly magnetized wells. Despite this, the disappearance of $SrTiO_3$ magnetism with increasing well thickness connects ferromagnetic spin correlations in the $SrTiO_3$ wells with the local order parameter destabilized at the quantum critical point in this system [11].

The temperature dependence of the ordered moments within the wells tracks that of the ferrimagnetism within $GdTiO_3$ spacing layers, suggesting that the molecular field of neighboring $GdTiO_3$ polarizes moments within the wells. The induced phase is therefore distinct from the hysteretic response identified in prior magnetoresistance measurements with a lower characteristic temperature ($T_c \approx 5$ K). Either a nontrivial field dependence of the order induced within the wells or an alternative order parameter, such as orbital order, should be invoked to explain this low temperature state. Rather, our key finding is a striking realization of interface-induced magnetic polarization across nominally nonmagnetic $SrTiO_3$ quantum wells nearly 2 nm thick embedded within a Mott insulating $GdTiO_3$ matrix.

---

*stephendwilson@engineering.ucsb.edu

[1] S. Stemmer and S. J. Allen, Annu. Rev. Mater. Res. **44**, 151 (2014).

[2] P. Moetakef, T. A. Cain, D. G. Ouellette, J. Y. Zhang, D. O. Klenov, A. Janotti, C. G. Van de Walle, S. Rajan, S. J. Allen, and S. Stemmer, Appl. Phys. Lett. **99**, 232116 (2011).

[3] H. Y. Hwang, Y. Iwasa, M. Kawasaki, B. Keimer, N. Nagaosa, and Y. Tokura, Nat. Mater. **11**, 103 (2012).

[4] A. Bhattacharya, S. J. May, S. G. E. te Velthuis, M. Warusawithana, X. Zhai, B. Jiang, J.-M. Zuo, M. R. Fitzsimmons, S. D. Bader, and J. N. Eckstein, Phys. Rev. Lett. **100**, 257203 (2008).

[5] J. Y. Zhang, J. Hwang, S. Raghavan, and S. Stemmer, Phys. Rev. Lett. **110**, 256401 (2013).

[6] A. Vailionis, H. Boschker, Z. Liao, J. R. A. Smit, G. Rijnders, M. Huijben, and G. Koster, Appl. Phys. Lett. **105**, 131906 (2014).

[7] J. M. Rondinelli, S. J. May, and J. W. Freeland, MRS Bull. **37**, 261 (2012).

[8] C. A. Jackson, J. Y. Zhang, C. R. Freeze, and S. Stemmer, Nat. Commun. **5**, 4258 (2014).

[9] S. Stemmer and A. J. Millis, MRS Bull. **38**, 1032 (2013).

[10] J. Y. Zhang, C. A. Jackson, R. Chen, S. Raghavan, P. Moetakef, L. Balents, and S. Stemmer, Phys. Rev. B **89**, 075140 (2014).

[11] E. Mikheev, C. R. Freeze, B. J. Isaac, T. A. Cain, and S. Stemmer, Phys. Rev. B **91**, 165125 (2015).

[12] P. Moetakef, J. R. Williams, D. G. Ouellette, A. P. Kajdos, D. Goldhaber-Gordon, S. J. Allen, and S. Stemmer, Phys. Rev. X **2**, 021014 (2012).

[13] C. A. Jackson and S. Stemmer, Phys. Rev. B **88**, 180403 (2013).

[14] J. A. Borchers, J. F. Ankner, C. F. Majkrzak, B. N. Engel, M. H. Wiedmann, R. A. Van Leeuwen, and C. M. Falco, J. Appl. Phys. **75**, 6498 (1994).

[15] B. J. Kirby, J. W. Lau, D. V. Williams, C. A. Bauer, and C. W. Miller, J. Appl. Phys. **109**, 063905 (2011).

[16] T. S. Santos, B. J. Kirby, S. Kumar, S. J. May, J. A. Borchers, B. B. Maranville, J. Zarestky, S. G. E. te Velthuis, J. van den Brink, and A. Bhattacharya, Phys. Rev. Lett. **107**, 167202 (2011).

[17] See Supplemental Material at http://link.aps.org/supplemental/10.1103/PhysRevLett.117.037205, which includes Refs. [18–21], for additional experimental and modeling details, supporting analysis, and supplementary reflectometry data.

[18] B. Jalan, R. Engel-Herbert, N. J. Wright, and S. Stemmer, J. Vac. Sci. Technol. A **27**, 461 (2009).

[19] P. Moetakef, J. Y. Zhang, S. Raghavan, A. P. Kajdos, and S. Stemmer, J. Vac. Sci. Technol. A **31**, 041503 (2013).

[20] B. Kirby, P. Kienzle, B. Maranville, N. Berk, J. Krycka, F. Heinrich, and C. Majkrzak, Curr. Opin. Colloid Interface Sci. **17**, 44 (2012).

[21] J. Lynn and P. Seeger, At. Data Nucl. Data Tables **44**, 191 (1990).

[22] J. F. Ankner, C. F. Marjkrzak, and S. K. Satija, J. Res. Natl. Inst. Stand. Technol. **98**, 47 (1993).

[23] F. Ott, J. Phys. Condens. Matter **20**, 264009 (2008).

[24] C. Majkrzak, K. O'Donovan, and N. Berk, in *Neutron Scattering from Magnetic Materials*, edited by T. Chatterji (Elsevier Science, Amsterdam, 2006), pp. 397–471.

[25] H. D. Zhou and J. B. Goodenough, J. Phys. Condens. Matter **17**, 7395 (2005).

[26] P. Moetakef, D. G. Ouellette, J. Y. Zhang, T. A. Cain, S. J. Allen, and S. Stemmer, J. Cryst. Growth **355**, 166 (2012).

[27] J. Y. Zhang, C. A. Jackson, S. Raghavan, J. Hwang, and S. Stemmer, Phys. Rev. B **88**, 121104 (2013).

[28] S. Stemmer and S. J. Allen, Annu. Rev. Mater. Res. **44**, 151 (2014).